Mechanochromism, Shear Force Anisotropy, and Molecular Mechanics in Polydiacetylene Monolayers

A. R. Burns, R. W. Carpick†, D. Y. Sasaki, J. A. Shelnutt§*
Sandia National Laboratories, MS 1413
Albuquerque, NM 87185-1413

R. Haddad
Department of Chemical Engineering
University of New Mexico
Albuquerque, NM 87131.

Abstract

We use scanning probe microscopy to actuate and characterize the nanoscale mechanochromsim of polydiacetylene monolayers on atomically-flat silicon oxide substrates. We find explicit evidence that the irreversible blue-to-red transformation is caused by shear forces exerted normal to the polydiacetylene polymer backbone. The anisotropic probe-induced transformation is characterized by a significant change in the tilt orientation of the side chains with respect to the surface normal. We also describe a new technique, based on shear force microscopy, that allows us to image friction anisotropy of polydiacetylene monolayers independent of scan direction. Finally, we discuss preliminary molecular mechanics modeling and electronic structure calculations that allow us to understand the correlation of mechanochromism with bond-angle changes in the conjugated polymer backbone.

* Corresponding author: aburns@sandia.gov, (505)-844-9642, FAX (505)-844-5470
† Current address: Department of Engineering Physics, University of Wisconsin-Madison, 1500 Engineering Dr., Madison, WI 53706-1687.
§ Also: Department of Chemistry, University of New Mexico, Albuquerque, NM 87131

Keywords: atomic force microscopy, friction force microscopy, friction anisotropy, shear force microscopy, nanotribology, polydiacetylenes, LB films, molecular mechanics, conjugated polymers
Running title: "Polydiacetylene Monolayers"

1. Introduction

As evidenced by other articles in this issue, organic films of ordered, densely-packed molecules have been used extensively as model lubricants to study the structural, mechanical, and chemical aspects of adhesion and tribology. In most cases, these films are monolayers of simple alkanes, of variable chain length and tail group chemistry, that are created either by self-assembly or Langmuir-Blodgett (LB) techniques [1, 2]. Considerable insights have been obtained concerning the effects of alkane chain ordering and packing on friction as measured by atomic force microscopy (AFM) [3-8]. Another class of organic thin films, polydiacetylenes (PDA), not only have a high degree of alkane chain ordering, but also incorporate a cross-linked conjugated backbone that exhibits a chromophoric response to stress and molecular rearrangement ("mechanochromism") [9]. PDA films have been examined as *in situ* optical transducers of applied stress [9, 10], chemical binding [11], and thermally-induced phase transformations [12, 13]. In addition, they have many unique structural properties, integral to the chromic behavior, that result in friction anisotropy [14, 15] and shear-induced molecular rearrangement [9].

In Fig. 1, we show the basic structure of a PDA monolayer. The linear conjugated backbone is parallel to the LB subphase following UV polymerization of the ordered monomer phase, and retains this geometry when transferred to the substrate surface. Thus it is bound to the substrate *via* an interaction with the head groups on the lower set of side chains, while the upper set of side chains and tail groups becomes the "interface" with probe tips, analytes, solvents, *etc.* The lengths of the side chains and the chemistry of the head and tail groups can be modified much in the same manner as for the model lubricant alkanethiols or silanes [11, 16-19].

The intense optical absorption characteristic of PDA, and of conjugated polymers in general [20-22], is caused by the excitation of π electrons in the extended linear backbone. Both absorption and fluorescence (if any) in the visible region tend to be highly polarized along the backbone direction. We have shown that high quality films exhibit large domains of crystalline alignment on the basis of strong polarization extinction [9]. The chromatic transition of PDA

DISCLAIMER

absorption from the visually "blue" form to the "red" form is not fully understood, but is generally associated with "strain" imparted to the conjugated backbone by the side chains [23]. The blue form is thought to be in the ordered "rod-like" geometry where the side chains are in the same plane as the backbone, which permits extended, continuous π overlap or "conjugation length" [24-27]. Out-of-plane conformational disorder in the side chains disrupts the π overlap and hence shortens the conjugation length, which in turn shifts the absorption spectrum to higher energy of the red form. However, the exact correlation between the conformational geometry and the electronic structure remains elusive. We address this problem by using molecular mechanics and electronic structure calculations. The problem is further complicated by AFM analyses on thermally [28] and shear-induced [9] blue-to-red transformations in PDA trilayers that revealed no obvious evidence of side chain disordering.

In our earlier study of mechanochromism in PDA trilayers [9], we presented results consistent with the notion of side chain rotation out of the backbone plane. However, that study was restricted to trilayers, since LB monolayers of our 10,12-pentacosadiynoic acid monomer precursor are not stable on a pure water subphase. We found that the shear-induced blue-to-red transformations were complicated by the removal of the top bilayer, revealing an seemingly "flattened" monolayer underneath. Thus aspects of molecular conformation changes in the mechanochromism were obscured by the trilayer geometry. It became clear that stable monolayer films were required to simplify characterization of the shear-induced molecular structure changes associated with the nanoscale mechanochromism. In Part 3.1 of this report, we describe compelling evidence of side chain rotation in the mechanochromism actuated by AFM probe tips on a stable PDA monolayer. The monolayer was formed by the polymerization of N-(2-ethanol)-10,12-pentacoasdinamide [19] (structure A in Fig. 1). The stability is due to inter-chain H-bonding at the head groups (Fig. 1). It should be noted that AFM friction anisotropy of the photochromic red form (as made on the LB trough with excess UV light) of these monolayers has already been published [14].

In Parts 2 and 3.2, we discuss a new technique that allows us to examine friction anisotropy in PDA films that, unlike our earlier AFM work [14], is independent of scan direction. It takes advantage of the directionality of the lateral oscillation motion used in shear-force microscopy [29-32]. The preliminary results indicate that the technique does work and offers many possible advantages to the study of molecular-level friction.

We present preliminary results of our molecular mechanics and electronic structure calculations in Part 3.3. Here we use 12 repeating unit energy-minimized structures of PDA, one made from each of the monomers discussed above, on which we perform full molecular mechanics at 300 K for 500 psec. The resulting conformational changes in the backbone, particularly dihedral angles induced by side chain movement, are then correlated with the calculated electronic structure and absorption spectra. In this way we are able to determine minimum conformational changes for color shifts.

2. Experimental

2.1 Sample preparation

Si substrates with either native or thermally grown oxide were cleaned in organic solvents followed by a 50/50 mixture of H_20_2 and 30% H_2S0_4 for 20 minutes at 100°C, then immediately rinsed and stored in pure water before transfer to the LB trough. AFM images indicated very little observable contamination and verified that the substrates were extremely flat, with < 2Å RMS roughness. Just prior to monolayer spreading, the substrates were removed from water storage and completely immersed into the trough subphase, minimizing exposure to air. The Si substrate was seated horizontally approximately 1 mm below the subphase surface.

PDA monolayers were prepared via UV polymerization on the LB trough that rests on a vibration isolation table inside a class 100 clean room. The pure water subphase had a resistivity greater than 18 MΩ cm and was held at a temperature of 15±1°C. The monomer N-(2-ethanol)-10,12-pentacoasdinamide (structure A in Fig. 1) was prepared as described elsewhere [19] and dissolved in 50% chloroform/benzene for dropwise spreading on the subphase. All films were

equilibrated for 20 minutes at 20 mN/m, prior to UV light exposure from a pair of Hg pen lamps whose output is dominated by the 254 nm and 365 nm lines. To produce a uniform blue film, the pen lamps were fixed 15 cm from the compressed monolayer (23 μW/cm^2) and switched on for 30 seconds. Photochromic red films were produced by placing the lamps 10 cm from the monolayer (40 μW/cm^2) and exposing it for 5 minutes. Transfer of the blue or red films was accomplished by slowly lowering the polymerized film onto the horizontal Si substrate by draining the trough. Samples were dried in clean room air and stored in a dark, nitrogen-purged container. A PDA sample that is made red by excess UV irradiation on the trough is referred to as a "photochromic" red sample; otherwise, we refer to the red form as that which is mechanically or thermally converted from the blue form after transfer to the substrate.

2.2 AFM and directional shear force microscopy

The AFM (Nanoscope IIIA, Digital Instruments) was operated under ambient conditions with a single silicon nitride cantilever and tip. We used the nominal force constant of 0.06 N/m for the calculated loads. More scanning details are discussed in Sec. 3.1.

The directional shear force experiment is shown schematically in Fig. 2. It is part of a near field scanning optical microscope based on the design described by Stranick *et al.* [33]. For the present purposes only the shear-force feature is discussed here. An optical fiber is mounted concentrically with respect to the four quadrant "dither" piezo (EBL#1, 0.125 inch diameter, 0.18 inch long) by gluing it inside a short 24-gauge stainless tube that is held by a metal clip (not shown) in a ceramic cap on the piezo. The end of the optical fiber is HF-etched to form a 200 μm conical taper with tip diameter of approximately 100 nm [34]. The optical fiber has mechanical resonances in the 12-30 kHz range for fiber lengths of about 1.5 mm protruding from the metal tube, and a Q of 60-90 before contact. The lateral motion amplitude of the fiber is determined by $A_{piezo}Q$, where $A_{piezo}$is the piezo drive amplitude (1.23 nm/V). The piezo is driven by a sinusoidal voltage applied to two adjacent quadrants (*e.g.*, +y,-x in Fig. 2), and fiber motion is detected by phase-sensitive lock-in amplified voltages induced on the other two quadrants (*e.g.*, +x,-y).

Details and variations on this very sensitive technique have been published elsewhere [32, 33, 35, 36]. We use a sinusoidal drive voltage of ±10 mV with respect to the grounded inner electrode, which results in a tip lateral motion amplitude of $A_{piezo}Q$= 1 nm for Q= 80. The unique aspect of this technique is that the direction of the lateral motion can be changed by switching to new drive and detection quadrants. Thus as shown in Fig. 2, we can change the direction by 90° by switching to +y,+x drive quadrants (detect with –x,-y). Hardwired switching is the method we use here, but electronic, continuously variable direction control is under development.

The frequency response of the fiber-piezo system is shown in Figs. 3 and 4 for the orthogonal drive directions +y,+x and +y,-x, respectively. In each figure we show the detected piezoelectric signals (B, lower) and the simultaneous lock-in detected signal of laser light scattered off the fiber tip (A, upper). The laser is used as a initial check to determine which are true fiber resonances. The angle of the laser beam is 45° with respect to both drive directions to insure equal signal strength when the drive direction is switched (see Fig. 2). (Because the optical signals are much weaker and noisier relative to the piezoelectric signals, this data was taken with a drive amplitude of ±56 mV.) Also, in the upper right of each figure is a CCD image of the moving tip under 800X magnification, showing the actual drive direction at the strongest peaks and drive amplitude of ±40 V.

One can see that the piezo-detected signals have a dispersive appearance, as noted previously by Brunner, *et al.* [36]. As they point out, this effect is most likely due to the interference of the tip resonance signal with the background signal coming from the drive piezo. We can model that as follows. The equation of motion for a damped harmonic oscillator can be given by:

$$\ddot{x} + 2\beta\dot{x} + \omega_0^2 = A\cos\omega t \tag{1}$$

where x is the displacement at frequency ω, β is the damping term, A is the driving force, and ω_0 is the resonance frequency. A possible solution to Eq. 1 is:

$$x(t) = D\cos(\omega t - \theta) \tag{2}$$

where, θ is the phase shift of x with respect to A, and D is the amplitude of x. Substituting Eq. 2 into Eq. 1 one obtains:

$$\left\{A - D\left[\left(\omega_0^2 - \omega^2\right)\cos\theta + 2\omega\beta\sin\theta\right]\right\}\cos\omega t - \left\{D\left[\left(\omega_0^2 - \omega^2\right)\sin\theta - 2\omega\beta\cos\theta\right]\right\}\sin\omega t = 0 \quad (3)$$

From Eq. 3, it can be shown that:

$$\sin\theta = \frac{2\omega\beta}{\sqrt{\left(\omega_0^2 - \omega^2\right)^2 + 4\omega^2\beta^2}}$$
$$\cos\theta = \frac{\omega_0^2 - \omega^2}{\sqrt{\left(\omega_0^2 - \omega^2\right)^2 + 4\omega^2\beta^2}} \quad (4)$$

$$\theta = \tan^{-1}\left(\frac{2\omega\beta}{\omega_0^2 - \omega^2}\right) \quad (5)$$

$$D = \frac{A}{\sqrt{\left(\omega_0^2 - \omega^2\right)^2 + 4\omega^2\beta^2}} \quad (6)$$

If there are no other mechanical resonances in the frequency region except that of the fiber, the amplitude D (Eq. 6) of the fiber interferes at a phase shift θ with the constant background C (normally subtracted) of the drive piezo, thus the detected amplitude D_{det} is given by:

$$D_{\text{det}} = C + D\cos\theta = C + \frac{\left(\omega_0^2 - \omega^2\right)A}{\left(\omega_0^2 - \omega^2\right)^2 + 4\omega^2\beta^2} \quad (7)$$

Re-plotting the first resonance at 13.9 kHz from Fig. 3, we see in Fig. 5 that Eq. 7 fits the data fairly well with ω_0= 13.936 kHz and β = 0.105. Also, $Q \cong (\omega_0/2\beta) = 66$, which is consistent with other measurements, including a fit of the optical signals with Eq. 6. To use this signal for shear-force feedback, we sit on the positive-going peak and feedback on a 10% attenuation. Thus for a ±10 mV drive, $A_{piezo} \cong 0.01$ nm, and we estimate from Ref. [32] that the shear force F at 10%

enuation is $F \cong A_{piezo}\, k(0.10) = 0.15$ nN, where $k = 150$ N/m is the spring constant of the glass er.

Molecular mechanics and quantum calculations

In the molecular mechanics (MM) calculations, two separate molecules were examined: one rminated with a carboxyl (COOH) head group and the other with the amide head group shown in g. 1. For each, a single, isolated all-trans PDA oligomer 12 units long (i.e., 12 sets of side-ains above and below the backbone) was sketched and minimized (10,000 iterations for the rboxyl and 2300 for the amide) using MM whereby it remained planar and ordered. The MM nd molecular dynamics (MD) were performed with PolyGraf software (Version 3.21) using a reiding II force field for atomic interactions. The dielectric constant was set to 2.64, and charges ere assigned using the charge equilibration method. A canonical MD simulation using the loover formalism was then setup for 500 ps with the temperature set at 300 K. Structures were etermined at fixed intervals (0.1 ps for the carboxyl head group, 0.25 ps for the amide). During ne simulation, the side chains became highly disordered and the backbones developed bends due o out-plane side chain rotations. Structures at the beginning (0 ps), end (500 ps), and several ntermediate times (occurring before and after some noticeable bends in the backbone) of the MD un, were then selected for quantum electronic structure calculations described below. To onsiderably simplify and shorten the quantum calculations, all side groups were "clipped" off, eaving methyl groups in their place. The hydrogens added to the methyl carbons were minimized sing MM while holding the backbone and methyl carbon positions fixed.

The electronic properties of the clipped conjugated backbone in its various configurations were alculated using ZINDO/S semi-empirical methods on the HyperChem 5.02 software package. INDO/S is particularly useful for predicting UV/visible spectra and can be parameterized to eproduce spectroscopic transitions when used with the CI (configuration interaction) single xcitations method. The quantum calculations gave the orbitals, energies, transition energies and ipoles.

3. Results

3.1 Mechanochromism of PDA monolayer

Before we discuss the AFM-induced blue-to-red transformation (mechanochromism) of the PDA monolayer, it would be useful to summarize what we previously determined on the trilayer [9]. We shall see that many of the trilayer observations are even more evident in the high-resolution images of the monolayer mechanochromism. Since the red form fluoresces and the blue does not, fluorescence microscopy of the transformed regions was used to verify that the mechanochromism occurred [9, 13].

(1) Defects in the film such as pinholes and crack edges assist significantly in the initial formation and growth of the red domains.

(2) The mechanochromism does not proceed without sliding contact occurring between the tip and sample; *i.e., shear forces are required.*

(3) The growth of the red domains is strongly anisotropic, with preferential growth along the backbone direction. Furthermore, the mechanochromism propagates along the backbone direction *beyond* the region where shear stress has been applied.

(4) The mechanochromism proceeds most rapidly when the sliding (fast scan) direction is perpendicular to the backbone direction. In most cases, it will not proceed at all when the fast scan direction is parallel to the backbone direction.

(5) Growth of the red areas proceeds faster at larger loads. Variation from sample to sample and even within one sample makes it difficult to quantify the exact load dependence of the mechanochromism rate. Imaging at very low loads (0 to -20 nN) in the absence of significant adhesion effectively provides a method of imaging the sample without promoting mechanochromism.

In Fig. 6, we show 1×1 μm^2 height and friction AFM images of blue and blue-to-red transformed monolayers near an area of bare silicon oxide substrate. The transformation took place during scanning at an estimated load of 6 nN and scan rate of 4.5 Hz. The images were subsequently acquired at a 0 to -20 nN load and 3 Hz rate. The red regions, particularly in the

friction image, reveal the backbone direction (indicated by the arrows) via striations that may be due to uneven packing density of the individual backbones [14]. As per observation (1) above, the presence of the bare "hole" in the blue film facilitated the mechanochromism. The red regions appear to nucleate at the edge of the hole and the growth of the domains is clearly along the PDA backbone [observation (3) above]. The scan direction is almost normal to the backbone direction in the upper region, which appears to have transformed to a greater extent (probably faster) than the lower region of the image [observation (4)].

From the molecular modeling calculations (Sec. 3.3) we estimate that the head to tail distance of the all-*trans* PDA (Fig. 1) is approximately 31.7 Å. AFM measurements under light imaging loads (0 to –20 nN, where no mechanochromism occurs) revealed a blue-form PDA film thickness of 27±3 Å and a photochromic red–form thickness of 31±3 Å [19]. Thus the nominal molecular tilt angle of the blue film is 30±10°, which is consistent with previously reported values of multilayer films [12, 37], and the photochromic red film has essentially 0° tilt. The photochromic red film is also more densely packed [19]. The blue regions in Fig. 6 are 22±2 Å thick (45±5° tilt) and the transformed red regions are 9±0.9 Å thick (74±2° tilt). *Thus it appears that the side chains are being pushed towards the substrate by the tip as it scans perpendicular to the backbone direction.* We depict this schematically in Fig. 6C. It is important to note that even though the morphology of the transformed red region is completely different from the closely-packed, upright morphology of the photochromic red films, the two red forms have identical fluorescence spectra [9] and comparable emission intensities. Thus we conclude that the overall polymer orientation and packing is not the cause of the mechanochromism or optical properties of the red films, but rather it is the stress on the backbone imparted by the re-oriented side chains that is the important aspect.

The friction in the red transformed regions increases up to 100% relative to the blue regions. Moreover, the lowest red PDA regions have the highest friction. Thus the friction appears to correlate directly with the compression or re-orientation of the side chains towards the surface. Much of the friction in the transformed regions is most likely due increased disorder of the

molecular packing. However, the re-orientation will also expose the side chain methylene ($-CH_2-$) groups and the conjugated backbone. Since these have a higher surface energy than the methyl (CH_3) tail groups [38], it is likely that a component of the higher friction is due to an increased adhesive interaction with the tip.

Clearly, if the AFM tip causes a re-orientation of the PDA molecules in the manner described above, they will need more room to accommodate the increased area per molecule. This is one reason why the mechanochromism is facilitated near bare spots and defects. This can also be seen in Fig. 7, where the backbone direction is parallel to the edge of the hole and almost perpendicular to the scan direction. Both aspects readily facilitated the mechanochromism, although we have no way of knowing if the PDA side chains were tilting towards or away from the bare region. The 1×1 μm^2 height and friction images were acquired *during* the transformation and represent "stills" from a long sequence of images: (A) and (C) under a 6 nN load and scan rate of 4.5 Hz, while (B) and (D) were acquired 28 frames later under an increased load of 17 nN. The transformation rate was observed to increase with higher load [observation (5)], but eventually decreased (at the same higher load) as the red region progressed farther from the bare substrate. Thus the molecules no longer "had the room" to re-orient at the same rate. Once again, the friction contrast is substantial between the red and blue regions.

3.2 Shear-force anisotropy

In the previous section we saw the critical importance of shear forces in the mechanochromism of the PDA monolayer. Elsewhere, we studied the friction anisotropy of a photochromic red PDA monolayer [14], and found that it also correlated with the backbone direction in a completely analogous dependence as the mechanochromism. In general, friction imaging is a potentially fruitful way to reveal structural aspects of thin films that may not show up in height images alone. In cantilever-based AFM lateral (friction) force measurements, it is not only necessary to have a sliding contact, but also the lateral force signal is optimized for a fast-scan direction 90° relative to

the axis of the cantilever. In this section, we will demonstrate that the friction anisotropy in the photochromic red PDA monolayer can also be seen using directional shear force microscopy.

As discussed in Sec. 2, directional shear force microscopy does not rely on the scan direction. Instead, we select the direction of the tip lateral motion by applying the drive voltages to different sectors of the dither piezo. Ideally, the mechanical resonance of the fiber should have one mode with a frequency independent of drive direction. However, due to the slight asymmetries in the way the optical fiber is glued into the metal tube and in the way the metal tube is clamped in the ceramic cap, multiple modes appear and there are significant shifts in the resonance frequencies when the drive direction is changed (Figs. 3 and 4). Some of the modes are circular or elliptical, but these can be avoided by selecting those that have the strongest optical scattering signal. The strongest features usually have equal (±5%) signal amplitudes for each drive direction, both in the piezo-electric signals and the optical signals.

In Fig. 8, we demonstrate the directional shear-force technique. First we collect an image A ($3.0\times2.4\ \mu m^2$) using the +y,-x drive direction at ±10 mV excitation of the 14.725 kHz mode as our shear force signal (10% damped under feedback). The lateral motion direction relative to the 0° scan angle is indicated by the arrow. Two contrasting domains can be clearly seen. We now acquire another image (B) under identical conditions at a scan angle of 90°. We see that the image has rotated 90°, but is otherwise unchanged. Thus the shear-force signal is not dependent on scan direction. We now raise the tip out of contact, switch to the +y,+x drive direction, tune to the 13.936 kHz mode, and bring the tip back into contact under 10% damped feedback. The 0° scan angle image C has reversed contrast relative to A and B. This contrast can only be due to shear forces because the topology is unchanged. We repeat the scan under 90° scan angle to acquire image D which has, again, only rotated the image relative to C.

It is important to note that in order to reveal structural friction anisotropy via directional shear forces, adhesion must be reduced as much as possible. Adhesion from isotropic chemical forces is expected to wash out contrast due to structural anisotropy. For this reason, all of the data was acquired with a hydrophobic glass tip that was coated with a monolayer of $CF_3(CF_2)_5(CH_2)_2$-$SiCl_2$

via vapor phase deposition [39]. Water layers are expected to be present under the ambient conditions of ~20% relative humidity. However, there was no evidence of capillary condensation between the tip and the PDA films. Thus the shear force contrast that we see is due to structural aspects of the photochromic red PDA monolayer, with negligible contributions from chemical forces [32, 40].

The images in Fig.8 were very "flat," *i.e.*, there were no apparent topological features to within a few Å. Thus the contrast between domains is purely due to lateral forces. Of course, in shear-force feedback microscopy, where the scanning piezo responds to maintain constant damping of the lateral amplitude, all "visible" features derive contrast through either height or friction or both. In purely friction contrast, the load changes in response to the feedback [31, 32]. One way to distinguish height from friction in the absence of significant adhesion is to change the direction of the lateral motion. Images that do show both friction contrast reversal and apparent topology are shown in Fig. 9 (all 2.4×2.4 μm^2). Here the top two images taken at the orthogonal lateral directions are very similar with various defects in the film (*e.g.*, black holes), except for the small domain in the lower right corner. In image A it appears lower, whereas in B it appears higher than the surrounding area. This contrast reversal must be due to the anisotropy in shear forces for that domain. We see similar behavior in the lower images, where the relatively dark low friction domain in the lower left corner of image C appears in image D to be faintly brighter than the surrounding area. (The white objects in C and D are polymer impurities that were not removed from the monomer solution by the 0.2μm filter [19] and became imbedded in the film. Occasionally they pop out leaving the black holes seen in A and B.) Finally we show in Fig. 10 two images, one for each lateral direction, of a region that has only topography contrast, with no discernable friction contrast. According to the line scan (C) below, these features are most likely bilayers (50-60 Å thick) on top of the monolayer. Therefore, measurements of true topography are not affected by changing the shear force direction.

The spatial resolution provided by the relatively broad tip is unfortunately inadequate to discern the structural basis for the friction anisotropy in these images. It is most likely that the backbone

direction and packing is at the root of our observations. Faint striations in the bright (high shear force) region of image A in Fig. 8 hint at backbone directions which are normal with respect to lateral direction of the probe tip; the same region is dark (low shear force) in image B for the case where the lateral direction of the probe tip is parallel to the backbone directions. Considerable improvement in lateral spatial resolution is required as this technique matures. Other refinements will include continuous tuning of the lateral direction, and simultaneous normal force sensing [31, 32] so that direction-dependent shear force *vs.* distance profiles can be acquired without scanning.

3.3 Molecular mechanics and electronic structure calculations

One of the primary motivations in using the PDA monolayers is the potential use of its mechanochromism as an optical transducer of side chain disordering, film defects, or shear forces. Much of the results presented above clearly indicate that the shear forces experienced by the scanning probes are due to an interaction with the side chains that alters the side chain orientation with respect to the original plane of the all-*trans* "blue" form. Out-of-plane rotations of the side chains will disrupt the π-orbital overlap or "conjugation length," causing a blue shift of the absorption.

In this section, we briefly discuss our initial efforts to determine quantitatively what the minimum angle changes are that result in the absorption shifts. As discussed in Sec. 2.3, we do this by applying molecular mechanics and dynamics to an isolated 12-unit oligomer at 300 K for 500 ps. The oligomer rapidly under goes many twists and rotations, resulting in a large array of side chain orientations *vs.* time. The thermal fluctuations of the isolated oligomer are expected, whereas in a close-packed film, the polymers would be stabilized by their neighbors. For this study, the fluctuations allow us to quantitatively sample the molecular geometries and corresponding electronic structures for various conformations. Structural analysis was performed on the molecular geometries determined at fixed intervals (0.1 ps for the carboxyl head group, 0.25 ps for the amide). For the structure at each time interval, eleven dihedral angles (between the

twelve units in the chain) were calculated along the backbone. The dihedral angles were measured from one C=C double bond to the next, as shown below:

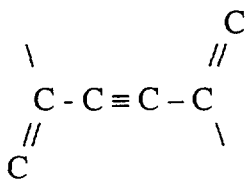

In the "dihedral angles" reported, the origin (0°) is set at what is traditionally defined as 180° since this is the starting (planar) configuration. This convention makes it easier to look at the deviations from planarity. The "average dihedral angle" is used as an index of overall deviation from planarity. The sign of the angles is unimportant, hence the average uses the absolute value. In Fig. 11, we show the average dihedral angle *vs.* time for the two oligomers with differing head groups. In the upper curve (A), the head group is COOH, that derives from the monomer 10,12-pentacosadiynoic acid, and does not make stable PDA monolayers. In the lower curve (B), the head group is the amide (see fig. 1A), that derives from the monomer N-(2-ethanol)-10,12-pentacoasdinamide, and does make stable PDA monolayers. In both oligomers we see significant deviations from planarity early on in the simulation. However, we also see smaller average dihedral angles at each time interval in the amide oligomer (B), due to hydrogen bonding between the head groups. The hydrogen bonding is also responsible for stabilizing the monolayer.

In Fig. 11, we also show a "clipped" oligomer (A) at t=128 ps, where the side chains have been replaced by methyl groups (see Sec. 2.3) *after* the MD simulation. The bent and clipped oligomer is used for the ZINDO/S quantum calculations on the conjugated backbone. In Fig. 12, we show the results from those calculations on the clipped oligomers from curve A of Fig. 11 at various times during the MD simulation. For visualization purposes, absorption spectra are generated from summing Lorentzian curves of oscillator strengths about the HOMO-LUMO singlet transitions; thus the line shapes and widths are arbitrary. We also do not make any assignments with regard to symmetry, so many of the transitions may not be allowed. Thus there are many more steps to be taken before we actually simulate the blue and red form absorption spectra.

However, the important information with regard to the present work is the *blue shift* in the spectra due the change in π-orbital energies during the MD simulation. One can see in Fig. 12 that there is a definite blue shift with increasing average dihedral angle (values taken from Fig. 11, curve A). We also see that there is a rapid shift from t=0 to t=80 ps, and essentially no shift after 200 ps. It is important to note that these spectra are instantaneous "snap shots" rather than averages, thus there can be large fluctuations in line position with time (*e.g.*, see spectra at 200 ps).

The blue shift in the spectra are caused by breaks in the π-orbital overlap that shorten the conjugation length. Thus, instead of using an average dihedral angle, another index is the "maximum conjugation length," which for a certain critical angle γ measures the longest sub-chain (within the whole 12 unit chain) present that is not "broken" by an angle greater (absolute value) than γ. In this way, we can see what critical angle is required to break conjugation in a way that shifts the absorption spectrum, and what the maximum conjugation length is during the simulation for that critical angle. The results are shown in Fig. 13 for a few selected γ. We see that by t<5 ps in the MD simulation there are already rotations <5°, and the conjugation length drops from the initial 12 units to 4, followed by a gradual change to 2 units over the next 200 ps. If we compare this to the spectral shifts in Fig. 12, we see that those shifts clearly have a different time dependence and must have required $\gamma >> 5°$; thus we can rule out very small dihedral angles from our analysis. Similarly, for $\gamma < 80°$, there is essentially no change in the conjugation length before 50 ps, yet we see significant spectral shifts before 50 ps. Thus we conclude that the conjugation is broken for angles smaller than 80°. (γ greater than 90° will tend to "re-form" conjugation as they approach 180°, and perhaps theoretically should not be counted as "breaking" the conjugation. In our computations, however, this effect was neglected since our dynamics simulation did not go on for long enough for it to become significant.) For $20° < \gamma < 60°$, the analysis becomes some less obvious. If we assume that the shift is crudely linear from 0-80 ps and rapidly levels off after t=80 ps, then the "best fits" appear for critical angles γ in the range 40°-60°, and that the conjugation length for the "red form" is < 6 units.

We conclude this section by noting that we can use the above analysis as a rough guide to morphological *changes* are required to observe mechanochromism. Clearly more detailed analysis is required, including nearest-neighbor and substrate effects. The photochromic red form appears to be highly ordered and densely packed [13, 14, 19, 37], thus we certainly cannot conclude that it has side chains rotated by 50° at least once every 6 units. However, we can conclude that very small changes in the blue form morphology are insufficient for mechanochromism, which is consistent with the AFM results discussed above and those reported earlier [9], and is consistent with the 18 kcal/mole activation energy [13] required for thermochromism.

4. Conclusions

We have presented a multi-faceted research effort in the area of conjugated polymer surfaces, specifically polydiacetylene (PDA), and how they may used to gain insight into molecular-level tribology. We have used synthetic strategies to develop stable, highly-ordered monolayers on atomically-flat substrates. PDA films that were initially in the all-*trans*, planar "blue form," characterized by its visual color, were interrogated with AFM techniques that triggered the mechanochromic transformation to the fluorescent "red form." The transformation was analyzed in detail and found to be dependent on the shear forces exerted on the pendant side chains. Those shear forces perpendicular to the backbone direction were most effective in the transformation, which was also facilitated by defects and neighboring areas of bare substrate. Overall, the transformation was the result of significant side chain rotation towards the substrate. Friction anisotropy was also observed and shown to directly correlate with the backbone direction. We showed that the anisotropy can be observed in a new way that takes advantage of directional lateral motion of shear-force microscopy that is independent of scan direction. Finally, we presented preliminary modeling results that will help us correlate the molecular structure changes such as side chain rotation with the color changes of the PDA films. So far we find that dihedral angle deviations from the blue planar form must be in the range of 40°-60° in order to see shifts in the absorption spectra for isolated molecules.

Figure Captions

Fig. 1: (A) Diacetylene monomer N-(2-ethanol)-10,12-pentacoasdinamide. (B) Ordering of monomers under 20 mN/m pressure on LB trough, followed by UV polymerization into (C) polydiacetylene (PDA). The H-bonding between the head groups is highlighted, although it is much weaker than the other bonds shown. The PDA monolayer is transferred *via* the head groups to the hydrophilic SiO_2 substrate.

Fig. 2: Schematic of directional shear-force experiment. An optical fiber is mounted concentrically in a four-quadrant piezo tube. The lateral motion of the fiber in one direction is caused by applying drive voltages to two adjacent quadrants (*e.g.*, +y,-x pair); motion orthogonal to this direction is produced by switching the drive to the +y,+x pair. A laser beam (dotted line) detects motion for either direction and is used only to identify tip resonances.

Fig. 3: Frequency response of tip lateral motion for drive voltages applied to +y,+x quadrants. (A) As detected optically by laser light scattering. (B) As detected piezoelectrically with quadrants (-y,-x). (Inset) CCD image of tip viewed end on showing direction of motion.

Fig. 4: Frequency response of tip lateral motion for drive voltages applied to +y,-x quadrants. (A) As detected optically by laser light scattering. (B) As detected piezoelectrically with quadrants (-y,+x). (Inset) CCD image of tip viewed end on showing direction of motion.

Fig. 5: Normalized frequency response data (open circles) from piezoelectric signal of Fig. 3 replotted under different scaling, and compared to theory (solid line) discussed in text.

Fig. 6: Height (A) and friction (B) images (1×1 μm^2) of region that was transformed under AFM shear forces. Arrows indicate backbone directions. The fast scan direction is along the x-axis.

The original blue (brightest in A, darkest in B) and transformed red regions are labeled as well as the bare substrate (darkest in A, brightest in B). The heights of the blue and red areas relative to the substrate are 22±2 Å and 9±0.9 Å, respectively. (C) Schematic representation of blue-to-red transformation.

Fig. 7: Consecutive height and friction images (1×1 μm^2) acquired *during* blue-to-red transformation by AFM shear forces. (C) and (D) were acquired 28 frames after (A) and (B) at scan rate of 4.5 Hz. The arrow indicates backbone direction and the blue, red and substrate areas are marked. See text for details.

Fig. 8: Directional shear force images (3.0×2.4 μm^2) of one region of a photochromic red PDA monolayer. (A) With +y,-x drive (direction shown at top with respect to image) and 0° scan angle. (B) Same as (A), except 90° scan angle. (C) With +y,+x drive (direction shown at top with respect to image) and 0° scan angle. (D) Same as (C), except 90° scan angle.

Fig. 9: Directional shear force images (all 2.4×2.4 μm^2, 0° scan angle) of two regions of a photochromic red PDA monolayer. (A) First region with +y,-x drive (direction shown at top with respect to image). (B) Same region, except with +y,+x drive (direction shown at top with respect to image). (C) Second region with +y,-x drive direction. (D) Same region, except with +y,+x drive direction.

Fig. 10: Directional shear force images (all 1.5×1.2 μm^2, 0° scan angle) of one region of a photochromic red PDA film. (A) With +y,-x drive (direction shown at top with respect to image). (B) Same region, except with +y,+x drive (direction shown at top with respect to image). (C) Line scan across middle of image (A).

Fig. 11: Calculated average dihedral angles *vs.* time from the molecular mechanics and dynamics simulation at 300 K. Curve A is for the 12-unit oligomer with the COOH head group, and curve B is for the amide head group (see text). Upper left we show an oligomer after 128 ps (curve A) that has been "clipped." The clipping takes place *after* the simulation and is used to simply the quantum calculations.

Fig. 12: Absorption spectra from the ZINDO/S quantum calculations for clipped oligomers at various times during the MD simulation. The arbitrary Lorentzian line shapes and widths are for visual purposes only. Also shown is the average dihedral angle from Fig. 11 for the oligomer at the specified time.

Fig. 13: "Conjugation length" of oligomer vs. time during the MD simulation. The length, which for a certain critical angle γ, measures the longest sub-chain (within the whole 12 unit oligomer) present that is not "broken" by an angle greater (absolute value) than γ.

Acknowledgements

R.W.C. acknowledges the support of the Natural Sciences and Engineering Research Council of Canada. Sandia is a multiprogram laboratory operated by Sandia Corporation, a Lockheed Martin Company, for the United States Department of Energy under Contract DE-AC04-94AL85000.

References

[1] A. Ulman, Introduction to Ultrathin Organic Films from Langmuir-Blodgett to Self-Assembly (Academic Press, New York, 1991).

[2] L. H. Dubois and R. G. Nuzzo, Annu. Rev. Phys. Chem. 43 (1992) 437.

[3] X.-D. Xiao, J. Hu, D. H. Charych and M. Salmeron, Langmuir 12 (1996) 235.

[4] A. Lio, D. H. Charych and M. Salmeron, J. Phys. Chem. B 101 (1997) 3800.

[5] H. I. Kim, T. Koini, T. R. Lee and S. S. Perry, Langmuir 13 (1997) 7192.

[6] H. I. Kim, M. Graupe, O. Oloba, T. Koini, S. Imaduddin, T. R. Lee, *et al.*, Langmuir 15 (1999) 3179.

[7] R. W. Carpick and M. Salmeron, Chem. Rev. 97 (1997) 1163.

[8] E. Barrena, S. Kopta, D. F. Ogletree, D. H. Charych and M. Salmeron, Phys. Rev. Lett. 82 (1999) 2880.

[9] R. W. Carpick, D. Y. Sasaki and A. R. Burns, Langmuir 16 (2000) 1270.

[10] R. A. Nallicheri and M. F. Rubner, Macromolecules 24 (1991) 517.

[11] D. H. Charych, J. O. Nagy, W. Spevak and M. D. Bednarski, Science 261 (1993) 585.

[12] A. Lio, A. Reichert, J. O. Nagy, M. Salmeron and D. H. Charych, Journal of Vacuum Science & Technology B 14 (1996) 1481.

[13] R. W. Carpick, T. M. Mayer, D. Y. Sasaki and A. R. Burns, Langmuir 16 (2000) 4639.

[14] R. W. Carpick, D. Y. Sasaki and A. R. Burns, Trib. Lett. 7 (1999) 79.

[15] M. D. Mowery, S. Kopta, D. F. Ogletree, M. Salmeron and C. E. Evans, Langmuir 15 (1999) 5118.

[16] S. Okada, S. Peng, W. Spevak and D. Charych, Acc. Chem. Res. 31 (1998) 229.

[17] U. Jonas, K. Shah, S. Norvez and D. H. Charych, J. Am. Chem. Soc. 121 (1999) 4580.

[18] M. D. Mowery and C. E. Evans, J. Phys. Chem. B 101 (1997) 8513.

[19] D. Y. Sasaki, R. W. Carpick and A. R. Burns, J. Colloid Interface Sci. in press (2000).

[20] Z. G. Soos, D. S. Galvao and S. Etemad, Adv. Mater. 6 (1994) 280.

[21] F. Garnier, Acc. Chem. Res. 32 (1999) 209.

[22] J.-L. Bredas, J. Cornil, D. Beljohnne, D. A. Dos Santos and Z. Shuai, Acc. Chem. Res. 32 (1999) 267.

[23] H. Eckhardt, D. S. Boudreaux and R. R. Chance, J. Chem. Phys. 85 (1986) 4116.

[24] K. S. Schweizer, J. Chem. Phys. 85 (1985) 1156.

[25] K. S. Schweizer, J. Chem. Phys. 85 (1985) 1176.

[26] V. Dobrosavljevic and R. M. Stratt, Phys. Rev. B 35 (1987) 2781.

[27] G. Rossi, R. R. Chance and R. Silbey, J. Chem. Phys. 90 (1989) 7594.

[28] A. Lio, A. Reichert, D. J. Ahn, J. O. Nagy, M. Salmeron and D. H. Charych, Langmuir 13 (1997) 6524.

[29] E. Betzig, P. L. Finn and J. S. Weiner, Appl. Phys. Lett. 60 (1992) 2484.

[30] R. Toledo-Crow, P. C. Yang, Y. Chen and M. Vaez-Iravani, Appl. Phys. Lett. 60 (1992) 2957.

[31] A. R. Burns, J. E. Houston, R. W. Carpick and T. A. Michalske, Phys. Rev. Lett. 82 (1999) 1181.

[32] A. R. Burns, J. E. Houston, R. W. Carpick and T. A. Michalske, Langmuir 15 (1999) 2922.

[33] S. J. Stranick, L. J. Richter and R. R. Cavanagh, J. Vac. Sci. Technol. B 16 (1998) 1948.

[34] P. Hoffmann, B. Dutoit and R.-P. Salathe, Ultramicroscopy 61 (1995) 165.

[35] J. Barentz, O. Hollricher and O. Marti, Rev. Sci. Instrum. 67 (1996) 1912.

[36] R. Brunner, A. Bietsch, O. Hollricher and O. Marti, Rev. Sci. Instrum. 68 (1997) 1769.

[37] R. F. Fischetti, M. Filipkowski, A. F. Garito and J. K. Blasie, Phys. Rev. B 37 (1988) 4714.

[38] J. N. Israelachvili, Intermolecular and Surface Forces (Academic Press, London, 1992).

[39] T. M. Mayer, M. P. d. Boer, N. D. Shinn, P. J. Clews and T. A. Michalske, J. Vac. Sci. Technol. B in press (2000).

[40] C. D. Frisbie, L. F. Rozsnyai, A. Noy, M. S. Wrighton and C. M. Lieber, Science 265 (1994) 2071.

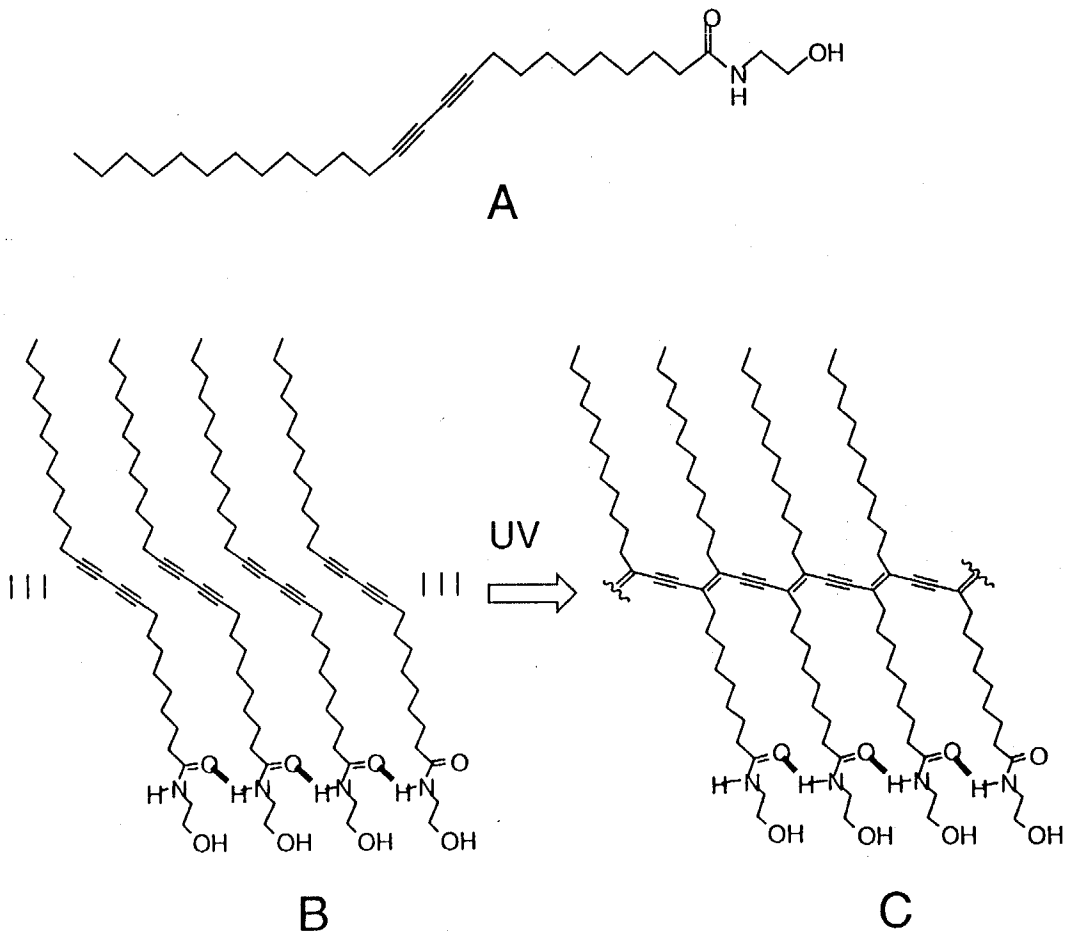

Fig. 1, Burns *et a/*

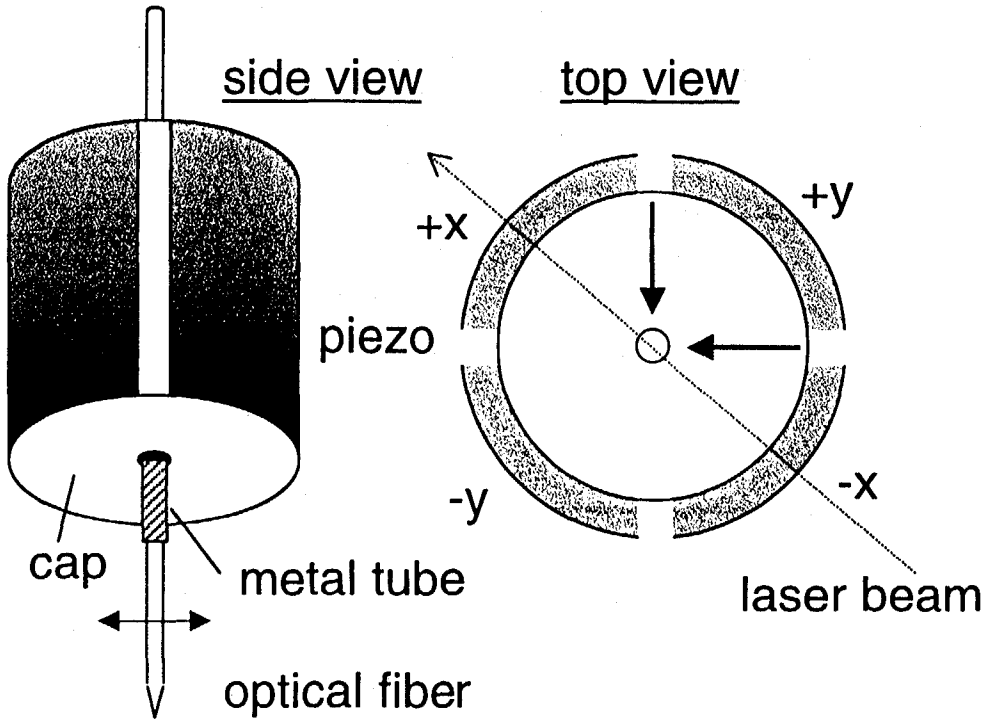

Fig. 2, Burns *et a/*

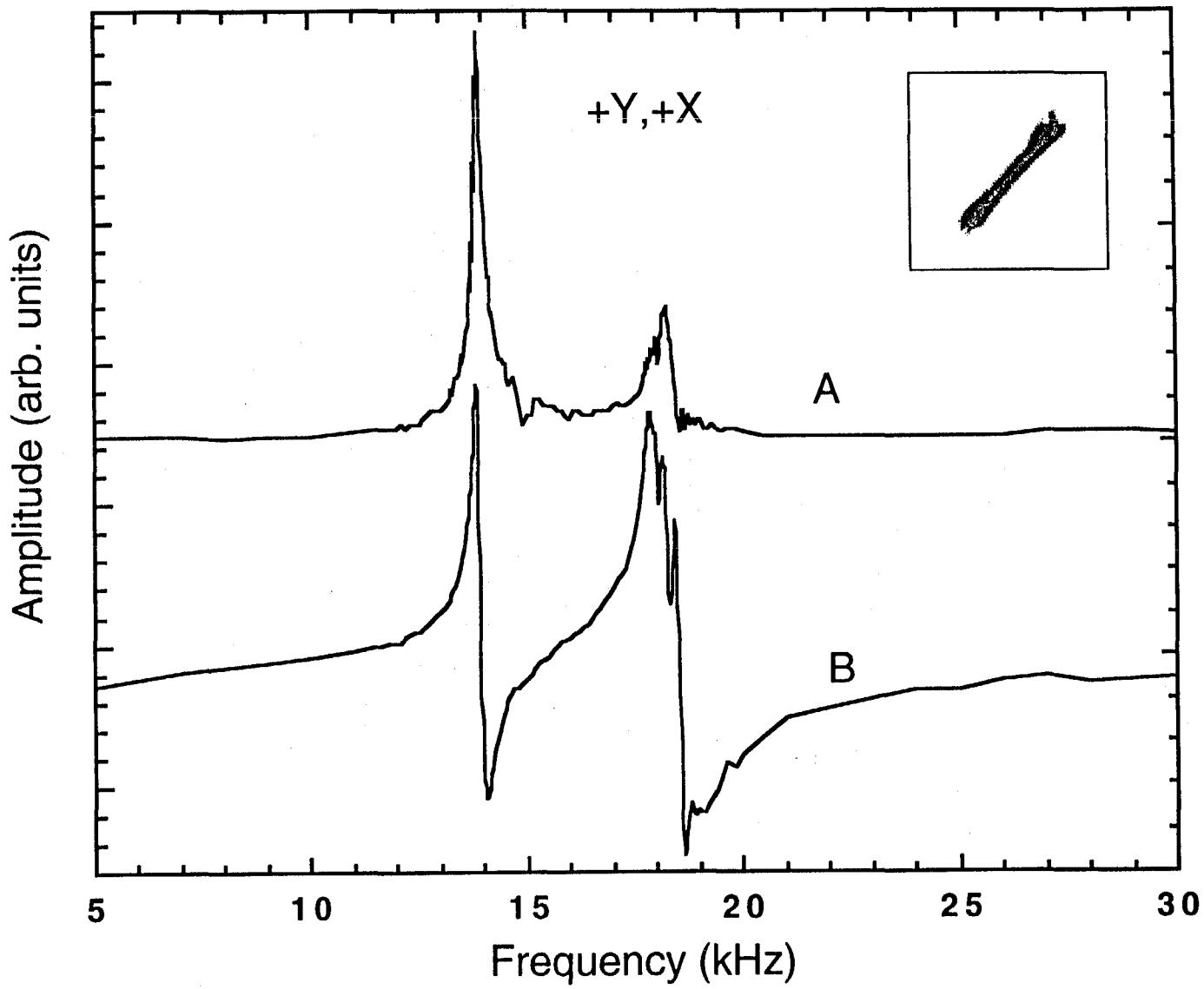

Fig. 3, Burns *et al*

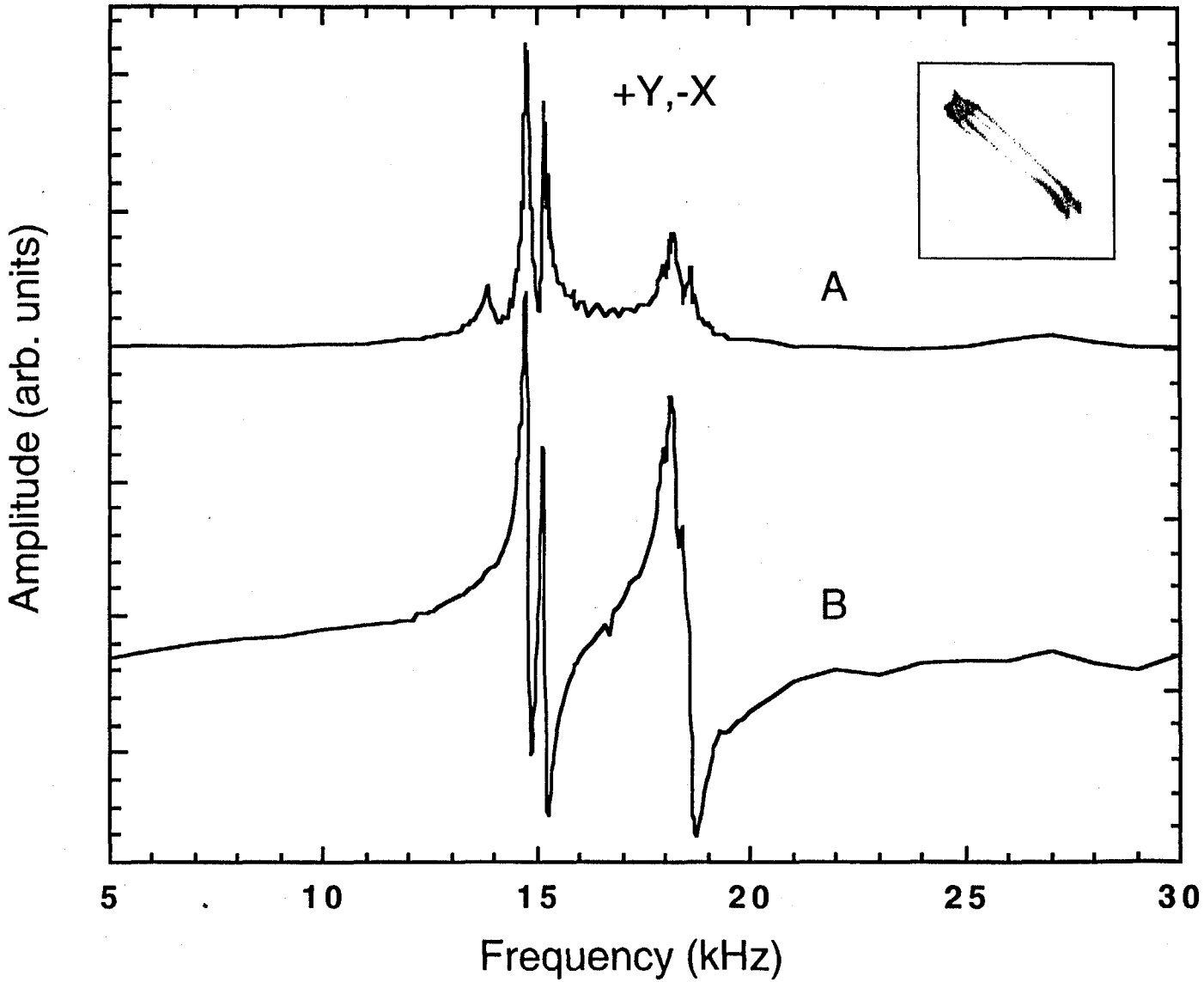

Fig. 4, Burns *et al*

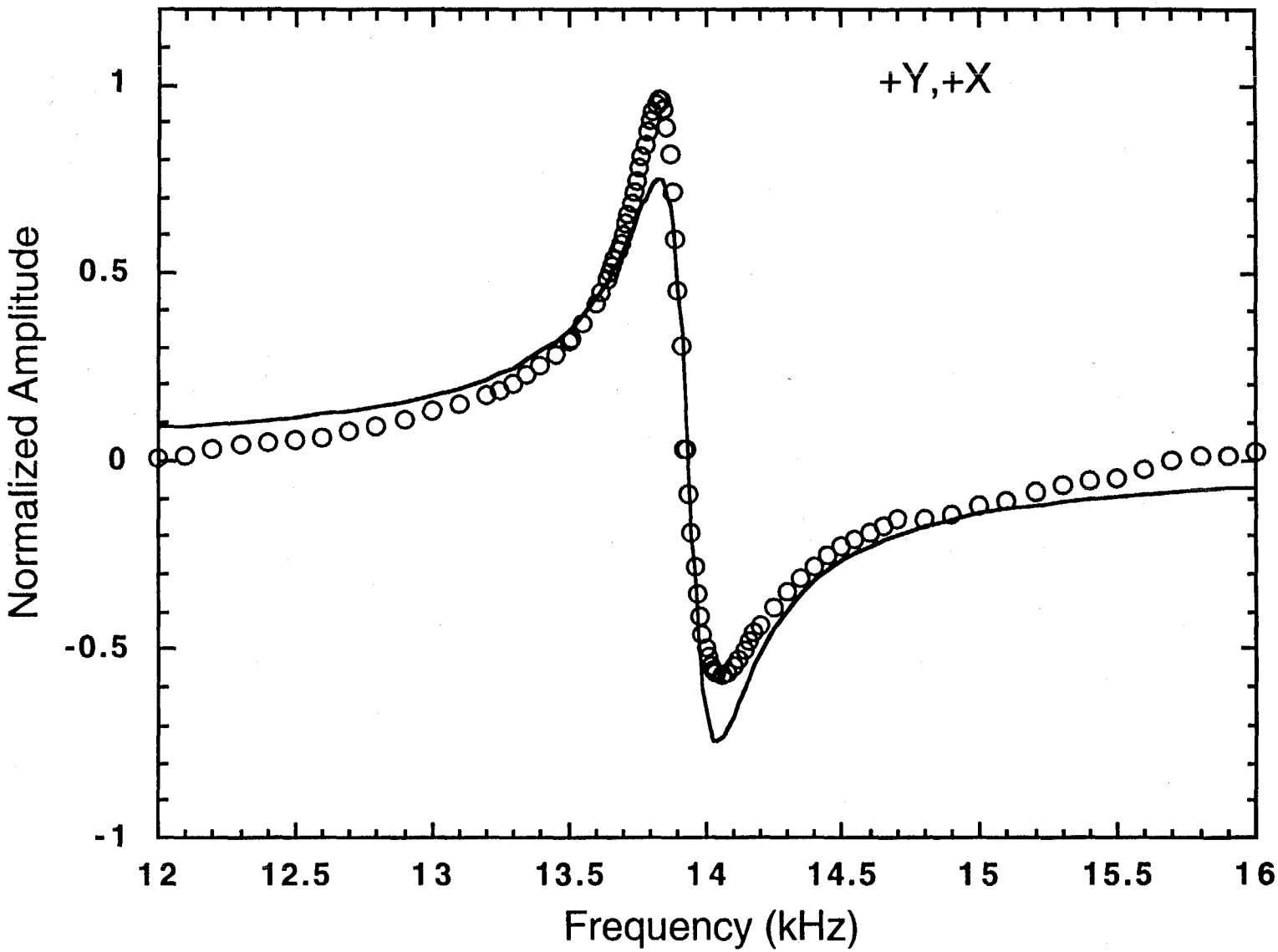

Fig. 5, Burns *et al.*

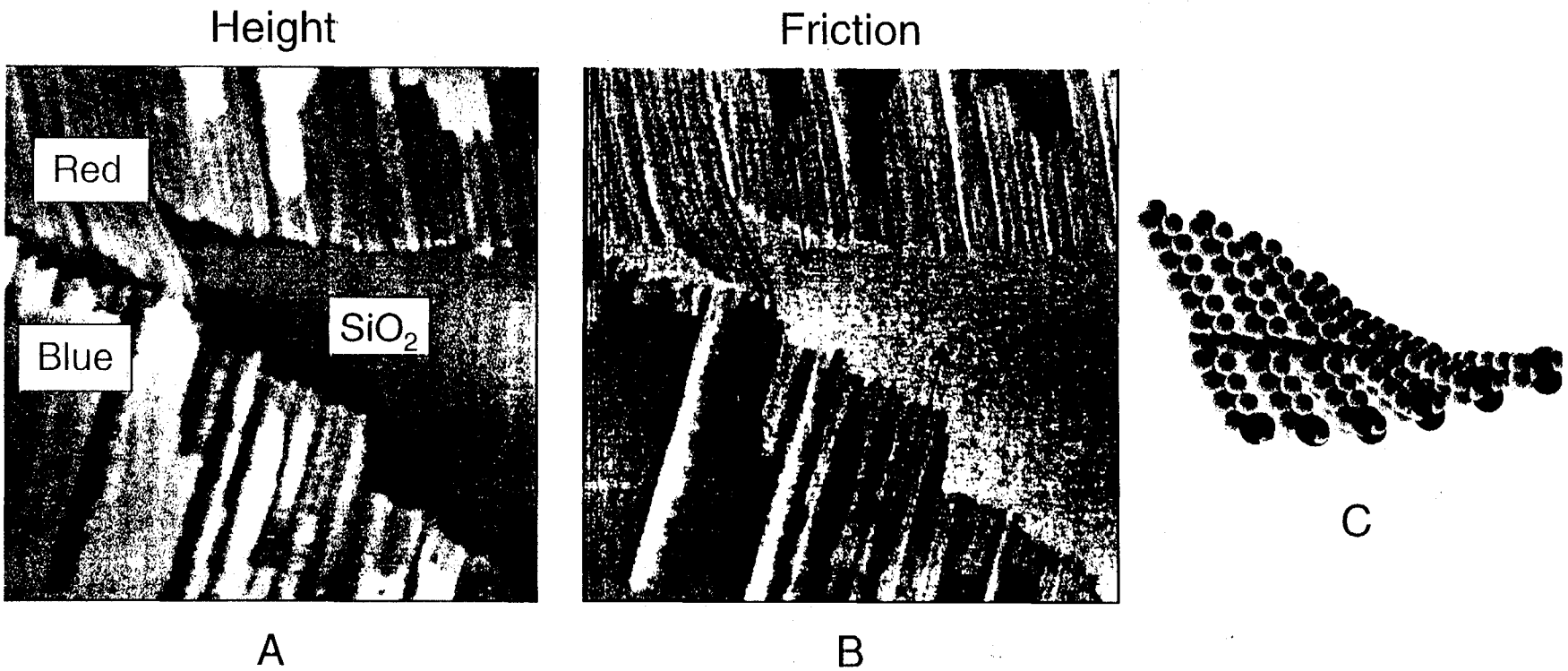

Fig. 6, Burns *et al*

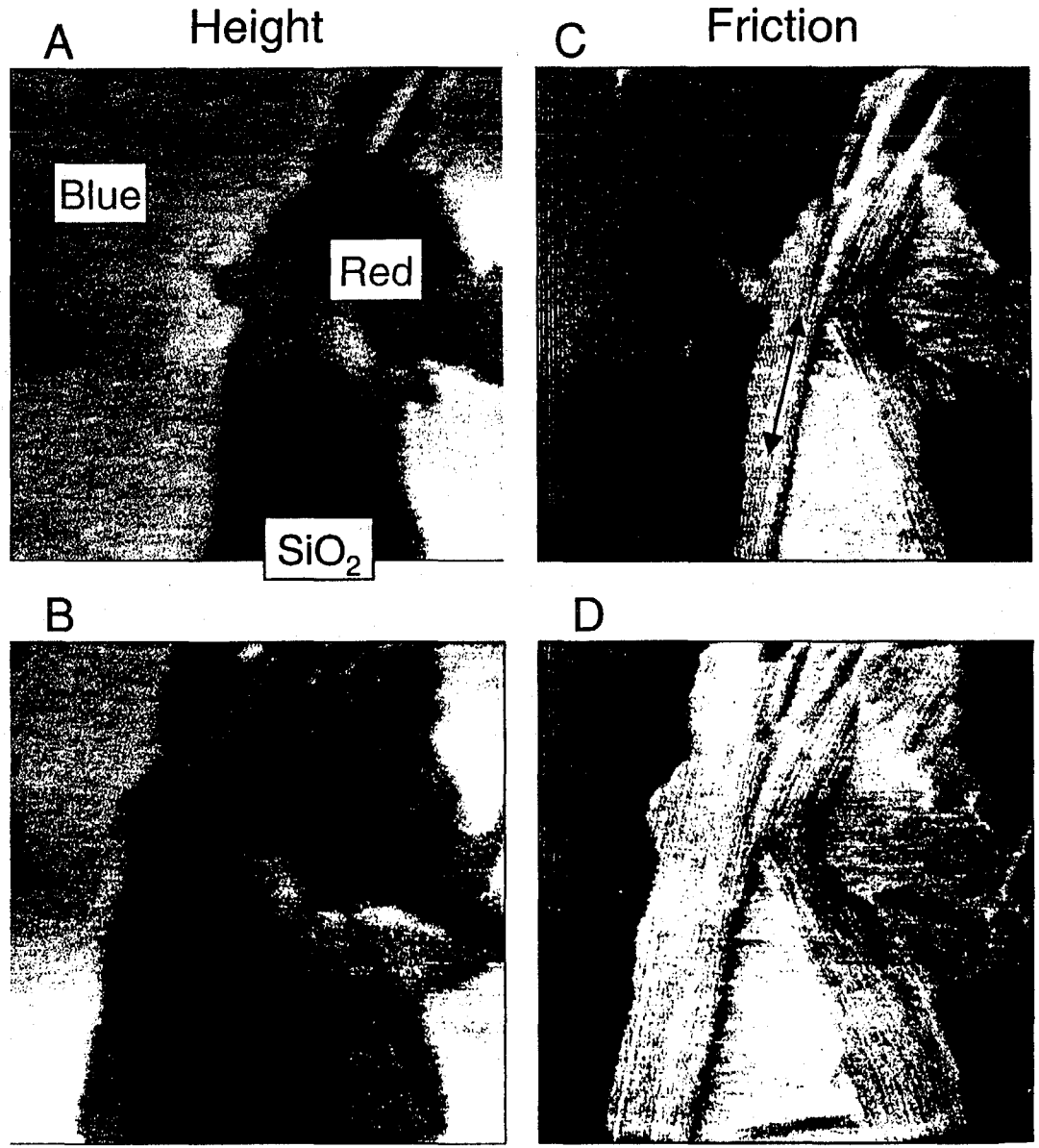

Fig. 7, Burns *et al*

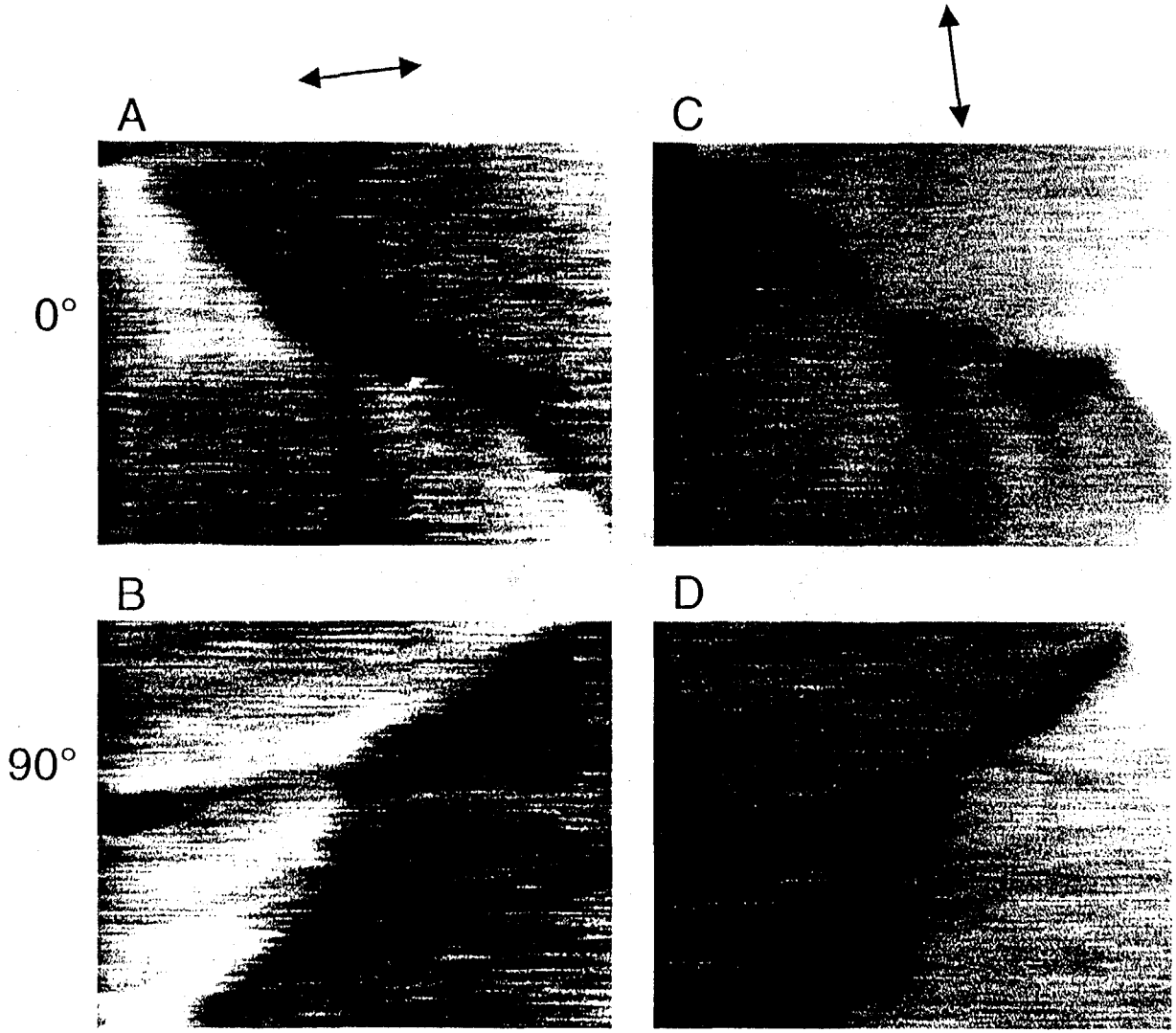

Fig. 8, Burns *et al*

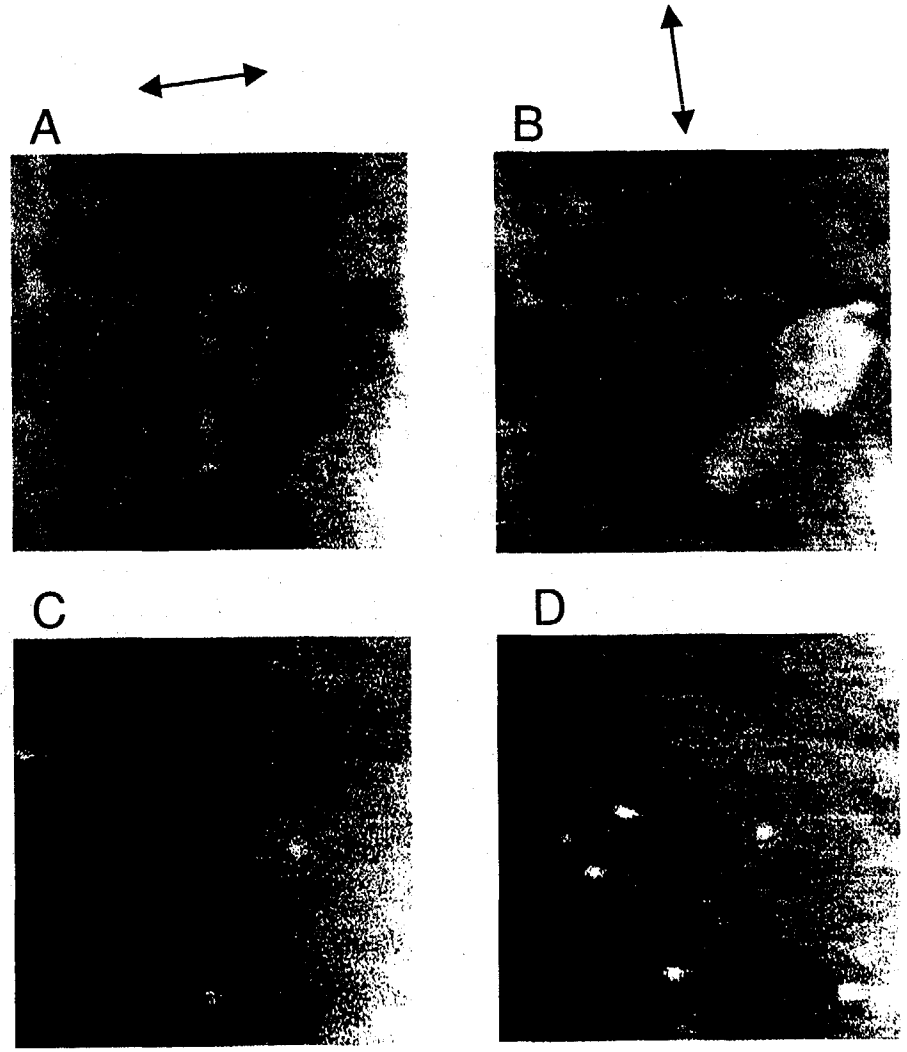

Fig. 9, Burns *et al*

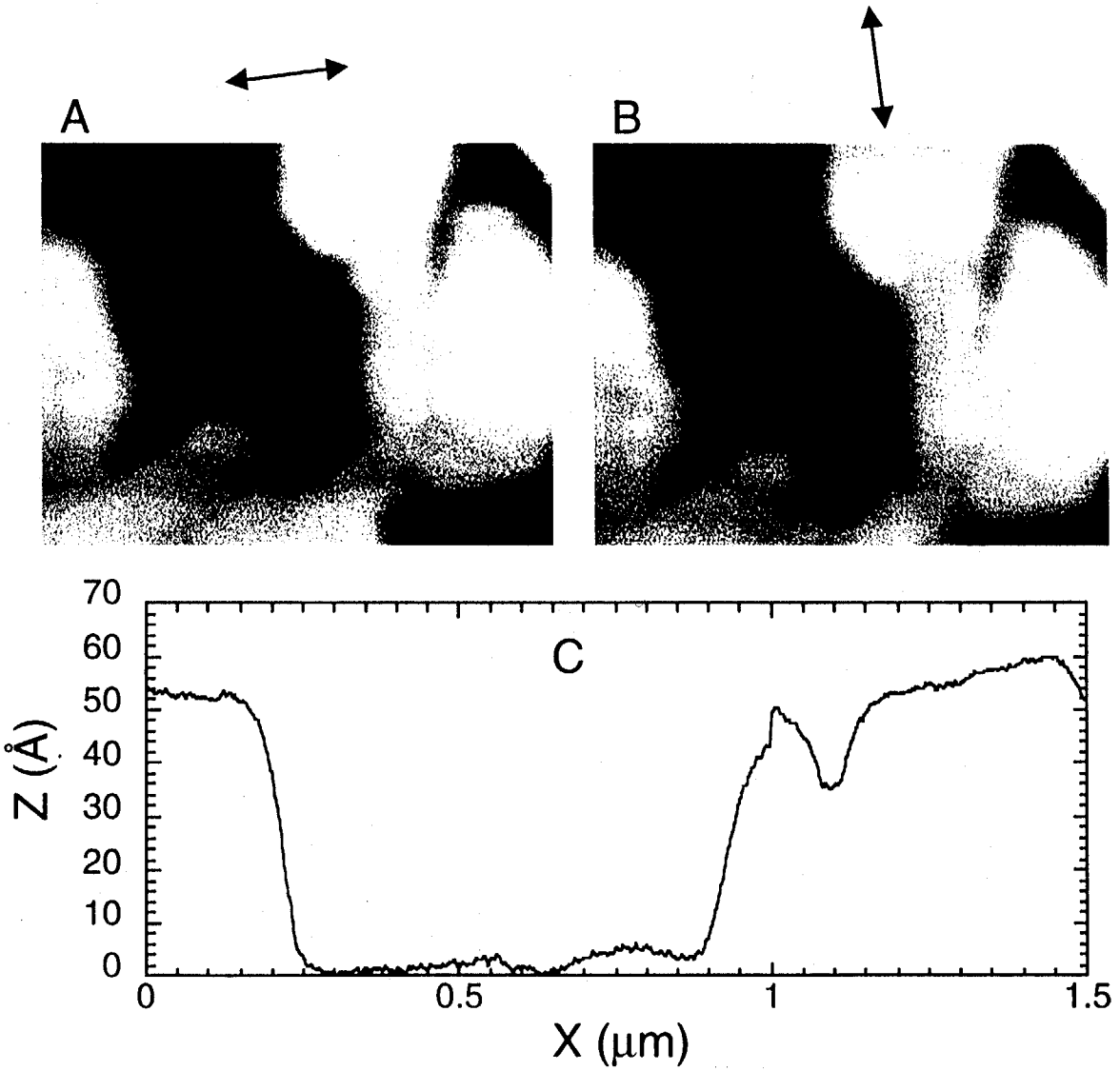

Fig. 10, Burns *et al*

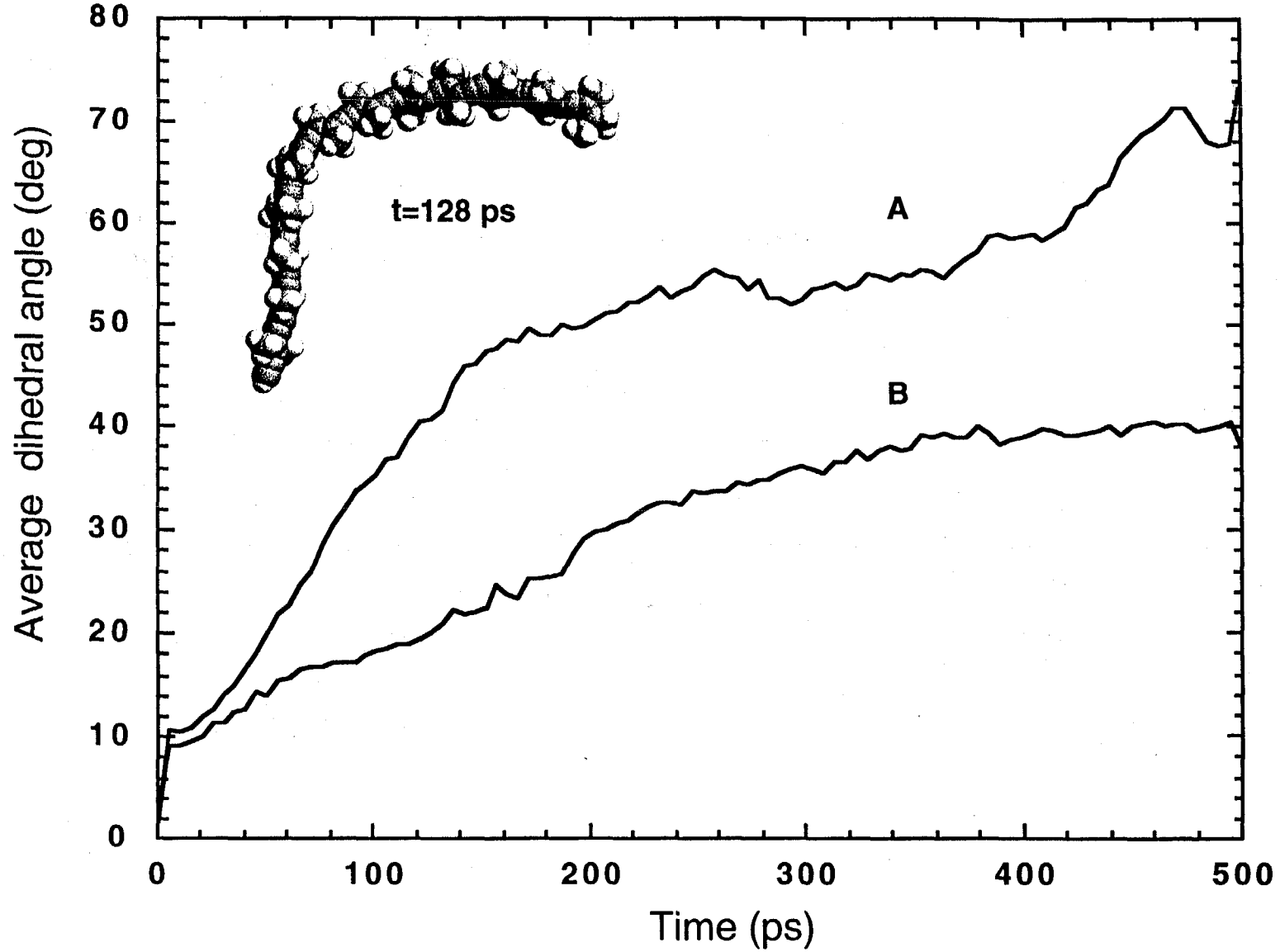

Fig. 11, Burns *et al*

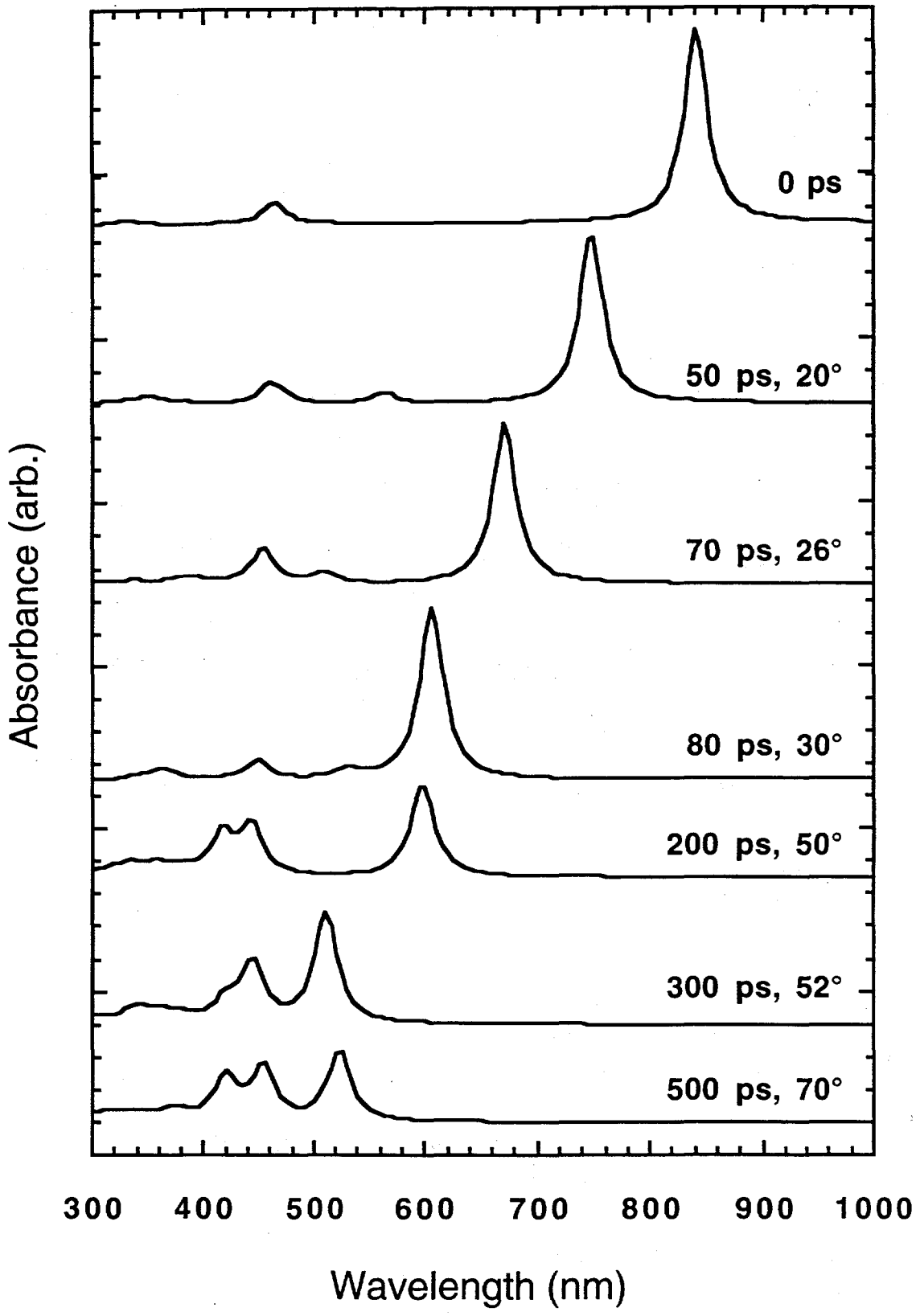

Fig. 12, Burns *et al.*

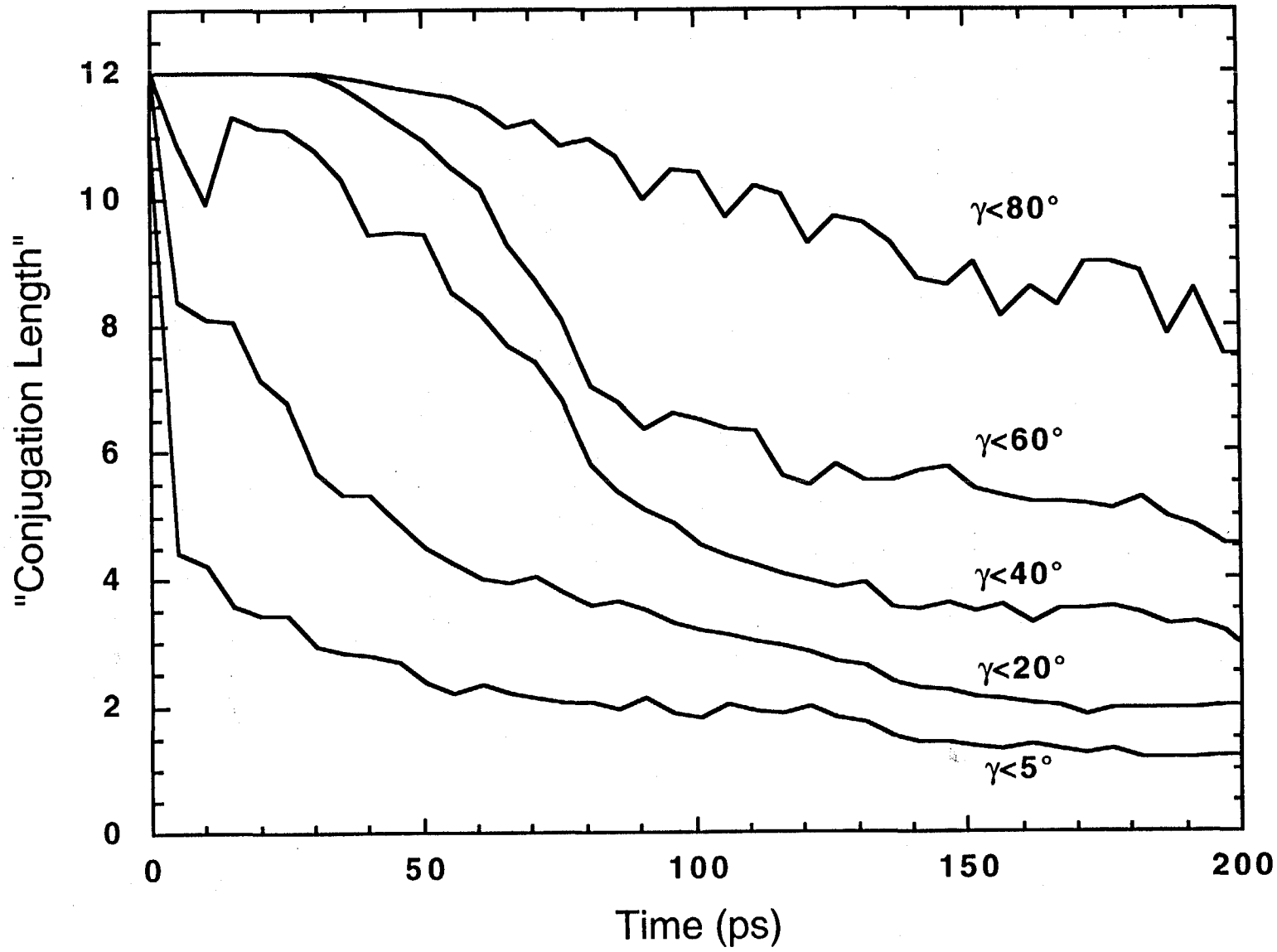

Fig. 13, Burns *et al*